# Lrig3 restricts the size of the colon stem cell compartment

Janelle G. Stevenson[1], Ryan Sayegh[2], Natalie Pedicino[3], Natalie A. Pellitier[4], Tim Wheeler[1], Matthew E. Bechard[6], Won Jae Huh[5], Robert J. Coffey[6,7,8,9], Anne E. Zemper[1]

[1]Department of Biology, Institute of Molecular Biology, University of Oregon, Eugene, OR 97403

[2]Department of Molecular, Cellular, and Developmental Biology, University of Colorado, Boulder, CO, 80309

[3]Department of Molecular, Cellular, and Developmental Biology, University of California Santa Cruz, Santa Cruz, CA 95064

[4]Department of Medicine, Oregon Health and Science University, Portland, OR 97239

[5]Department of Pathology, Yale School of Medicine, New Haven, CT, USA

[6]Department of Medicine, Vanderbilt University Medical Center, Nashville, TN 37232

[7]Department of Cell and Developmental Biology, Vanderbilt University Medical Center, Nashville, TN 37232

[8]Epithelial Biology Center, Vanderbilt University Medical Center, Nashville, TN 37232

[9]Department of Veterans Affairs Medical Center, Nashville, TN 37232

*Corresponding Author:
Anne E. Zemper, PhD
1229 University of Oregon
1318 Franklin Avenue
Room 273 Onyx Bridge
Eugene, OR 97403
Tel: 541-346-2403
Fax: 541-346-4854
E-mail: anniez@uoregon.edu

## Graphical Abstract

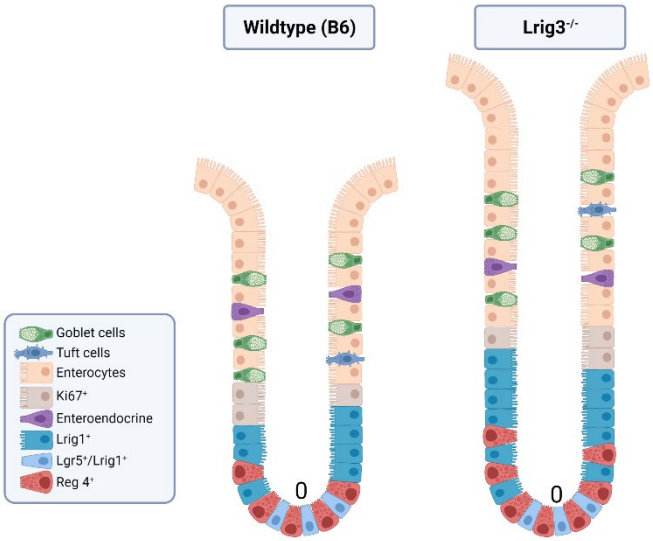



## Abstract

The cellular census of the colonic crypt is tightly regulated, yet the molecular mechanisms that regulate this census are not fully understood. Lrig3, a transmembrane protein, is expressed in colonic crypt epithelial cells, including the stem, progenitor, and differentiated cell types. Mice missing Lrig3 have a disruption in their cellular census: using a novel *Lrig3*$^{-/-}$ mouse we demonstrate that *Lrig3*$^{-/-}$ mice have more cells per crypt, a greater mucosal area, and longer colons compared to wildtype mice, suggesting the expression of Lrig3 is required for both the total number of epithelial cells in the mouse colon, as well as colon length. In addition, we show *Lrig3*$^{-/-}$ mice have significantly more stem, progenitor, and deep crypt secretory cells, yet harbor a normal complement of enteroendocrine, Tuft, and absorptive cells. *Lrig3*$^{-/-}$ mice also have a concomitant decrease in phosphorylated Extracellular signal-related kinases, indicating the loss of Lrig3 leads to an expansion of the colonic stem cell compartment, in an Erk-dependent manner. Our study describes the expression of Lrig3 within the colon, defines

45 perturbations in mice lacking *Lrig3,* and supports a role for Lrig3 in the establishment of
46 both colonic crypt structure and cellular census, defined as the epithelial cell type and
47 number in colon crypts.

48 **Introduction**

49 Precise spatiotemporal regulation of stem cell proliferation, differentiation, and
50 apoptosis are critical for proper regeneration of the gastrointestinal epithelium. In the
51 mouse colonic epithelium, the majority of cells are renewed every five days driven by
52 stem cell division at the base of the colonic crypt (10). In order to maintain crypt size and
53 epithelial cell number, the cellular census is tightly regulated by balancing the number of
54 stem, progenitor, and differentiated cells per crypt. We know that each of these cell types
55 are key for the absorptive and secretory jobs of the colon (13). Here, we evaluate how
56 the loss of Leucine-rich repeats and immunoglobulin-like domains 3 (*Lrig3*) affects crypt
57 cellular census and explore the impact of the loss of Lrig3 on these three critical cell types.

58 Lrig3 is a single-pass transmembrane protein and one of three members of the
59 Lrig protein family (22). Lrig family members generally regulate both receptor tyrosine and
60 serine/threonine kinases (22). To date, Lrig3 hasn't been as extensively studied as the
61 other Lrig family members, yet we know it is expressed across endo-, meso- and
62 ectodermal tissue types throughout embryonic development (8). Disruptions in Lrig3
63 affect proper neural crest formation in *Xenopus laevis* and result in incomplete formation
64 of the murine lateral semicircular canal (2, 30). Generally, mice, sheep and pig are smaller
65 if they have a loss-of-function in Lrig3 (1, 11, 15). Only recently have contributions to
66 primary literature uncovered mechanistic roles for Lrig3 in the progression of many cancer

67 cell types: cervical, hepatocellular, prostate, glioblastoma and colon (5, 6, 12, 17, 23, 24,
68 28).

69 While most adult vertebrates can survive and maintain some sort of
70 homeostasis with the loss of Lrig3, there are a number of defects that have been
71 described in knockout mice, including cardiac hypertrophy, misregulation of insulin levels
72 and the misorganization of neurons in the central nervous system (7, 11). In certain
73 tissues, Lrig3 works in concert with another family member, Lrig1 (7, 8). In the
74 gastrointestinal tract, Lrig1 is expressed on stem and progenitor cells in the small intestine
75 and colon and is functionally important for maintaining homeostasis. The loss of Lrig1
76 results in aberrant growth factor signaling and tumor formation (18, 25). From publicly-
77 available expression databases, we know Lrig3 is also highly expressed in the
78 gastrointestinal tract (32) and Lrig3 protein is predicted to have striking homology to Lrig1
79 (22). These reasons led us to hypothesize that Lrig3 is important for development and
80 homeostasis of the mouse colon. The goal of our study was to understand the impact of
81 the loss of Lrig3 on colon biology. Through transcript and protein expression analysis, we
82 show that Lrig3 is present throughout the colonic crypt epithelium, and we describe
83 multiple colon morphological and cellular defects in *Lrig3*$^{-/-}$ mice. Our study describes the
84 expression of Lrig3 within the colon, defines perturbations in mice lacking *Lrig3,* and
85 supports a role for Lrig3 in the establishment of both colonic crypt structure and cellular
86 census, defined as the epithelial cell type and number in colon crypts.

87 **Results**

88 **Lrig3 expression in colonic crypts**

89 Our first step was to define Lrig3 expression in the colonic crypts by assessing *Lrig3*
90 transcript and Lrig3 protein expression via *in situ* hybridization, immunofluorescence, and
91 western blot analysis, respectively. We generated an *Lrig3* knockout mouse (*Lrig3*$^{-/-}$, Fig.
92 1*A* and Supplemental Fig. S1) to both serve as a control for these analyses and to
93 evaluate the impact of the loss of *Lrig3*. Comparing wildtype (WT) tissue to *Lrig3*$^{-/-}$ tissue,
94 we observed *Lrig3* transcript expression in all colonic epithelial cells and this expression
95 was lost in the *Lrig3*$^{-/-}$ mice (Fig. 1*B-E*). Further, Lrig3 protein is expressed in the majority
96 of epithelial cells; this was confirmed by immunofluorescence and western blot analyses.
97 Lrig3 protein was absent in *Lrig3*$^{-/-}$ mice (Fig. 1*F-J*). These results define, for the first time,
98 Lrig3 expression in the mouse colonic crypt.

99 **_Lrig3_$^{-/-}$ mice have morphological and epithelial defects**

100 As our initial results demonstrate that Lrig3 is highly expressed throughout the colonic
101 crypt, we posited there may be epithelial disruption to the crypts in mice lacking *Lrig3*.
102 Indeed, initial survey of the colonic tissues indicated morphological differences, as well
103 as epithelial cellular census differences between WT and *Lrig3*$^{-/-}$ mice. To examine this
104 directly, we first assessed colon lengths, and found that adult *Lrig3*$^{-/-}$ mice have
105 significantly longer colons than WT mice at 6-10 weeks of age ($p<0.05$, Fig. 2*A*). We
106 hypothesized that along with the observed increase in colon length there may be
107 alterations at the cellular level. We examined this by measuring total mucosal area of WT
108 and *Lrig3*$^{-/-}$ mice using hematoxylin and eosin stained, paraffin-embedded tissue sections
109 and found that *Lrig3*$^{-/-}$ mice have a significantly larger mucosal area ($p<0.01$, Fig. 2*B-D*),
110 per tissue section. The larger mucosal area in *Lrig3*$^{-/-}$ mice could be for several reasons,
111 but we prioritized the investigation of two obvious hypotheses: 1) the epithelial cells within

112 *Lrig3*$^{-/-}$ mice are larger or 2) there are more cells present in the crypts of *Lrig3*$^{-/-}$ mice.
113 After an extensive examination of the colon sections from both sets of mice, we
114 determined there was no obvious difference in cellular size between the cohorts (data not
115 shown), ruling out that hypothesis. To investigate our second hypothesis, we quantified
116 the number of epithelial nuclei per crypt, across both cohorts, and found that *Lrig3*$^{-/-}$ mice
117 have more cells per colonic crypt than the WT mice ($p<0.05$, Fig. 2*E*). While there could
118 be many reasons for a greater number of cells, we first examined proliferation in the crypt
119 of *Lrig3*$^{-/-}$ mice compared to WT mice by quantifying the expression of Ki67, a proliferative
120 marker, in the epithelial cells. Surprisingly, we found no significant difference in the
121 number of proliferating epithelial cells in the colonic crypts of *Lrig3*$^{-/-}$ mice at 6-10 weeks
122 of age, compared to WT mice of the same age (Fig. 2*F-J*). From these analyses, we
123 conclude that *Lrig3*$^{-/-}$ mice have a greater number of cells per crypt, but these cells are
124 not undergoing aberrant proliferation.

125 **Colon crypt stem compartments are expanded in *Lrig3*$^{-/-}$ mice**

126 As epithelial cell number expansion is a hallmark of *Lrig3*$^{-/-}$ crypts, we wondered if this
127 increased cell number was attributed to a particular region of the crypt. As there are many
128 cell types present, we first assessed the stem and progenitor cells in the crypt-base by
129 examining *Lgr5* expression, as this is indicative of the presence of long-lived proliferative
130 stem cells in the base of the colonic crypt (4). First, we performed RNA Scope *in situ*
131 hybridization for *Lgr5* expression and identified significantly more *Lgr5*+ cells in the
132 colonic crypts of *Lrig3*$^{-/-}$ mice (Fig. 3*A-D*). In addition, some cells seemed to harbor
133 qualitatively more *Lgr5* than others, even in the WT tissue, consistent with previous
134 analyses of stem and progenitor markers in the gut (10). To more carefully examine this

135 observation, we devised a quantification scheme for looking at *Lgr5* transcript expression
136 levels in each cell. We binned them according to low- (<6 puncta per cell), mid- (6-14
137 puncta per cell), and high (15≤ puncta per cell) ranges (Fig. 3*E*). We quantified the puncta
138 in *Lrig3*$^{-/-}$ and WT cells and while we observed no difference in the number of *Lgr5* low-
139 expressing cells, there were significantly more mid- and high-expressing cells in *Lrig3*$^{-/-}$
140 mice ($p<0.001$, Fig. 3*F*). The other cell type present in the stem cell region of the crypt is
141 defined by the expression of the Reg4 protein. As Reg4+ cells act as support cells for
142 Lgr5+ cells (20), we reasoned that we may also observe a parallel increase in Reg4+
143 cells, in *Lrig3*$^{-/-}$ mice. To determine this, we quantified the number of Reg4+ cells and
144 found significantly more Reg4+ cells in the base of the crypt ($p<0.0001$, Fig. 3*G-K*). Reg4
145 is also expressed by secretory cells near the top of the crypt, thus we quantified the
146 number of Reg4+ cells in the upper half of the crypt and determined there is no change
147 in the number of these cells between *Lrig3*$^{-/-}$ and WT mice (Fig. 3*L*). Finally, we examined
148 the number of Vil-1+ (absorptive), Dclk1+ (Tuft), and ChgA+ (enteroendocrine) cells,
149 which correspond to three additional differentiated cell types found in the upper portion of
150 the crypts. Qualitatively, we found no obvious difference in Vil-1 expression, when
151 comparing approximately 50 images per genotype. Quantitatively, we found no difference
152 in Dclk1+ and ChgA+ cells when comparing *Lrig3*$^{-/-}$ and WT mice (Supplemental Fig. S2).
153 Collectively, our results demonstrate the increased cell number we observe in *Lrig3*$^{-/-}$ mice
154 is restricted to stem and support cells in the crypt base.

155 **_Lrig3_$^{-/-}$ mice have increased Lrig1 and decreased in pErk**

156 As the stem cell niche is expanded in *Lrig3*$^{-/-}$ mice, we next examined if there was any
157 change in expression of Lrig1, which is an Lrig3 family member, and widely expressed in

158 intestinal stem and progenitor cells(18). While Lrig1 is normally restricted to the crypt-
159 base, we found that *Lrig3*$^{-/-}$ mice have more Lrig1+ cells in the mid- and upper-crypt (Fig.
160 4*A-D*). We quantified the number of Lrig1+ cells per crypt and found significantly more
161 Lrig1+ cells in *Lrig3*$^{-/-}$ mice compared to WT mice ($p<0.0001$, Fig. 4*E*). We also quantified
162 Lrig1 expression in the crypts via western blot analysis and confirmed the increase in
163 Lrig1 we detected in *Lrig3*$^{-/-}$ mice (Fig. 4*F*). As loss of Lrig1 results in changes to growth
164 factor receptor signaling (18, 26), we next assessed if the over-expression of Lrig1 seen
165 in *Lrig3*$^{-/-}$ mice resulted in cell signaling changes in the crypts. We prioritized analysis of
166 total and activated Epidermal growth factor receptor (Egfr and pEgfr, respectively), as
167 these receptors are modulated based on Lrig1 expression (18). We also examined
168 extracellular signal-related kinase (Erk) expression, as this is a transcriptional activator of
169 proliferation and differentiation, and promoter of stemness in both the small intestine and
170 colon (16). We observed no obvious differences in the protein expression of total Egfr
171 (Fig. 4*G-H, K*), activated Egfr or total Erk (Fig. 4*I-K*); however, we consistently observed
172 decreased expression of phosphorylated Erk (pErk) in the *Lrig3*$^{-/-}$ colonic crypts by
173 western blot analysis (Fig. 4*K*). These results indicate this common downstream mediator
174 of mitogen activated kinase signaling is changed in mice lacking *Lrig3.* Taken together,
175 we observe that *Lrig3* is required for proper Lrig1 expression and appropriate Erk
176 activation.

177 **Discussion**

178 Using our novel *Lrig3*$^{-/-}$ mouse, we demonstrate that *Lrig3*$^{-/-}$ mice have more cells per
179 crypt, a greater mucosal area, and longer colons compared to wildtype mice. This
180 suggests the expression of Lrig3 is required for both the total number of epithelial cells in

181 the mouse colon, as well as establishment of colon length. Further, we show *Lrig3*$^{-/-}$ mice
182 have an Erk-associated expansion of the colonic stem cell compartment, as they harbor
183 significantly more stem, progenitor, and deep crypt secretory cells.

184 Our research defines the expression domain of Lrig3, in the colon for the first time,
185 as a novel marker of all colonic epithelial cells. The most well-studied Lrig family member,
186 Lrig1 (18), is a homologue of Lrig3 with redundant expression patterns in some tissues
187 (7, 8). In the colon, Lrig1 expression is distinct from that of Lrig3, as it is restricted to the
188 crypt-base (18, 26). As their expression patterns are distinct in the gastrointestinal tract,
189 it is likely that Lrig1 and Lrig3 also have unique molecular functions. *In vitro*, we know that
190 Lrig3 stabilizes the ErbB receptors, whereas Lrig1 promotes ErbB receptor degradation
191 (18). It is less clear if Lrig3 also promotes stabilization of ErbB receptors *in vivo*; this
192 observation may be tissue-dependent (3). As with Lrig1, Lrig3 has been evaluated across
193 many tissue types; and has a significant impact on growth factor receptor pathways. We
194 show that one common mediator of ErbB and Ras signaling pathways, Erk, is
195 dysregulated in *Lrig3*$^{-/-}$ mice. Through our examination of the ErbB family member, Egfr,
196 we did not observe any changes to expression or activation of this powerful growth factor
197 receptor in *Lrig3*$^{-/-}$ mice; the impact of Lrig3 loss on other growth cell signaling pathways
198 represents an important area of future research. Lrig3 also has been shown to regulate
199 fibroblast growth factor (FGF) receptors which results in changes to neural crest formation
200 in frog (30) and vascular endothelial growth factor (VEGF) receptors are modulated by
201 Lrig3 in glioma (17, 31). Both FGF and VEGF pathways are important for the development
202 and maintenance of the colonic epithelium (9, 21), but it is unknown if Lrig3 modulates
203 these pathways in this context. This represents an important area of future research.

204 The question of how Lrig3 is regulated may be equally as important as the question
205 as to what Lrig3 is regulating. Notably, *Lrig3* expression is directly modulated by miRNA-
206 196a, a microRNA that is upregulated in gastric, colon, breast and pancreatic cancer and
207 promotes tumorigenesis. In cervical cancer cells, miRNA-196a targets Lrig3 (19) and
208 improves cell viability. Lrig3 is also regulated at the post-transcriptional level, as there are
209 reports of a circular form of Lrig3 *(circRNA Lrig3*) that is highly expressed in human
210 hepatocellular carcinoma (HCC). Detection of blood plasma *circ-Lrig3* is a highly sensitive
211 and specific diagnostic indicator for HCC (23). Mechanistically, downregulation of
212 *circRNA Lrig3* represses both the MAPK/ERK and Smad pathways to prevent the
213 progression of HCC and the loss of *circRNA Lrig3* suppresses proliferation, invasion of
214 HCC cells *in vitro* and blocks tumor growth of HCC *in vivo* (12, 24). One recent report
215 gives us a glimpse of the potential role in advanced colon cancer. Using human colon
216 cancer cell lines, Zang and colleagues were able to show that Lrig3 represses metastasis-
217 associated cell motility by inhibiting slug via inactivating ERK signaling (29). While the
218 data on Lrig3 expression in solid tumors is expanding rapidly (5, 6, 12, 17, 23, 24, 29),
219 the role of Lrig3 in the gastrointestinal tract at the genome, transcriptional and protein
220 level is largely unknown and represents a valuable avenue for future research for both
221 normal and cancerous colon tissue.

222 In terms of the requirement for Lrig3 in colon development and homeostasis, we
223 have two key observations. The first is that *Lrig3*$^{-/-}$ mice are born physically smaller and
224 weigh less than their WT counterparts (11), yet we also consistently observe these mice
225 to have significantly longer colons at adulthood. While there has been a great deal of
226 research defining the molecular requirements for small intestinal morphogenesis, and to

227 some extent, for the colon (9, 13), our results clearly signify the importance of studying
228 Lrig3 and its role in colon development. While it is beyond the scope of this paper, a clear
229 next step to understanding how *Lrig3* impacts colon development is to take an *in vivo,*
230 inducible loss-of-function approach for Lrig3, using a timecourse strategy to define the
231 impact of loss of Lrig3 on birth weight and colon length.

232 Perhaps the most striking observation from our examination of *Lrig3*$^{-/-}$ mice is the
233 greater number of cells per crypt despite no significant change to proliferation, resulting
234 in *Lrig3*$^{-/-}$ mice having an expanded pool of stem and support cells in the crypt-base. While
235 colonic epithelial self-renewal has been extensively researched (10) the majority of this
236 research has been in adult mice, and generally has been assessed during regenerative
237 phases after tissue injury (27). From these studies, we know the key signaling pathways
238 that promote stem cell self-renewal and daughter cell differentiation (10). Cellular census
239 (epithelial cell type and number) is generally consistent from crypt-to-crypt in the distal
240 colon of both mice and humans. Unfortunately, there is a paucity of research examining
241 the molecular factors that regulate the number of colon cells and how the crypts arrive at
242 a homeostatic census (and thus a consistent crypt size) in adulthood. Our data clearly
243 demonstrate the requirement for proper Lrig3 expression to yield appropriate crypt cellular
244 census. Despite the increase in cell number per crypt in *Lrig3*$^{-/-}$ mice, we do not observe
245 an increase in all epithelial cell types. Indeed, we observe a specific increase in the
246 number of cells in the stem cell compartment at the crypt-base, suggesting that *Lrig3* is
247 critical for establishing the size of the stem cell compartment during development. In
248 future experiments, it will be important to test this hypothesis directly, either by
249 overexpression of Lrig3 or through forced, wide-spread regeneration of colon crypts in

250 *Lrig3*$^{-/-}$ mice. In the latter example, induction of acute injury to the adult *Lrig3*$^{-/-}$ colon to
251 spur crypt renewal will be instructive in understanding how *Lrig3*$^{-/-}$ mice arrive at this
252 aberrant state of homeostasis. Taken together, our results signify the importance of
253 studying Lrig3 and its role in cellular census and colon development.

254 **Experimental Procedures**

255 **Generating *Lrig3*$^{-/-}$ mice** – The *129 Lrig3* BAC clone (bMQ-129G9) was obtained from
256 Sanger Institute. The *Lrig3* targeting construct which disrupts exons 4-12 of the Lrig3
257 locus was generated by BAC recombineering (14). The gene disruption strategy, null
258 allele sequence and location of PCR primers is presented in Supplemental Figure 1. PCR
259 primer sequences are listed in Supplemental Table 1. ES cell electroporation and
260 subsequent blastocyst injections were performed by the Transgenic Mouse/ES Cell
261 Shared Resource at Vanderbilt University.

262 **Mice** – C57BL/6 and *Lrig3*$^{-/-}$ mice were housed in a specific pathogen-free environment
263 under controlled light cycle conditions, fed standard rodent lab chow, and provided water
264 *ad libitum*. All procedures were approved and performed in accordance with the University
265 of Oregon Institutional Animal Care and Use Committee. All mice were used at 6-10
266 weeks and mouse sex was mixed male to female at a roughly 50% ratio of each. All mice
267 were sacrificed by cervical dislocation. At time of sacrifice, colons were removed, flushed
268 with ice cold PBS and immediately measured using a ruler to obtain colon length, and
269 then bifurcated.

270 **Tissue Preparation for Staining** – Tissue for paraffin and frozen block preparation were
271 pinned onto a wax surface, fixed using 4% paraformaldehyde (PFA) for one hour (tissue

272 imaged in Fig1*G-J* were fixed in 4% PFA overnight), on a shaker at room temperature.
273 They were then washed three times (five minutes each) in PBS. For frozen blocks, tissue
274 was submerged 30% sucrose in PBS overnight at 4°C and embedded in optimal tissue
275 compound (OCT) for subsequent sectioning. For paraffin blocks, tissue was incubated in
276 70% ethanol and dehydrated in increasing alcohol baths and embedded in paraffin wax.
277 All slides were sectioned at 7μm, (unless stated otherwise), and stained according to
278 procedures below.

279 **Colonic Crypt Protein Isolation** – Bifurcated colons were cut into ~ 1cm pieces and
280 incubated in ice cold 2mM EDTA and 0.5mM DTT PBS buffer, washed in PBS, and
281 incubated 2mM EDTA buffer at 37°C. Tissue underwent vigorous lateral shaking to
282 release crypts from submucosa, suspension was decanted, and shaking was repeated
283 three times. The presence of single crypts is verified under a compound microscope and
284 residual submucosal tissue is removed. The final collection of crypt suspensions was
285 centrifuged at 500xg, cell pellet was then resuspended in Pierce RIPA buffer
286 (ThermoFisher) with protease (½ tablet, Pierce Protease Inhibitor Mini tablets, EDTA-
287 free, ThermoFisher) and phosphatase inhibitor (½ tablet PhosSTOP EASYpack, Roche),
288 homogenized using an 18-gauge needle, and centrifuged at maximum speed. The
289 supernatant was removed, and protein concentration determined using Pierce BCA kit
290 (ThermoFisher).

291 **Morphometric Analysis** – Mucosal area and nuclei per crypt were quantified using
292 paraffin embedded tissue and stained with Hematoxylin and Eosin (VWR). Images and
293 measurements were obtained on a Nikon Eclipse/Ds-Ri2. To quantify the mucosal area
294 we measured 10 images per animal (n=4 mice per genotype) using the Nikon NIS-

295 Elements measurement tool. We measured the area of colonic epithelium by drawing
296 lines across the basement membrane of the epithelium, along the sides, and across the
297 luminal edge. To quantify the nuclei per crypt we used Hematoxylin and Eosin-stained
298 paraffin slides and counted total nuclei per crypt in 10 images per animal (n=4 mice per
299 genotype).

300 **Antibodies and Staining Procedure** – Frozen tissue slides were washed in PBS three
301 times (three minutes each), blocked in 1% bovine serum albumin (BSA) and 0.03% Triton
302 X-100 suspended in PBS for 1 hour. Antibodies were diluted in this blocking buffer at
303 concentrations listed in Supplemental Table 1, applied to the sections and sections were
304 incubated overnight at 4°C. Slides were then washed in PBS three times (three minute
305 each) and incubated with secondary antibodies at 1:500 in the same blocking buffer as
306 above, for one hour at room temperature. Lastly, slides were washed in PBS for three
307 minutes, then washed in PBS plus DAPI (1:10,000) for five minutes, and finally washed
308 in PBS for three minutes. Slides were mounted using an n-propyl gallate/glycerol solution.
309 Paraffin slides underwent conventional deparaffinization in xylenes and rehydration via
310 ethanol washes and water, followed by antigen retrieval in a 1x Citrate buffer
311 (ThermoFisher) in a pressure cooker for one hour. Antibody catalog information and
312 concentrations used are listed in Supplemental Table 2.

313 **Western Blot** – Protein was diluted in a Laemmli buffer with 5% β-mercaptoethanol and
314 boiled at 95°C for five minutes. 25μg of protein was loaded per lane into an SDS-PAGE
315 gel (Bio-Rad Mini-Protean pre-cast gels 4-20%) and gels were run at 160V for
316 approximately 90 minutes. Protein was transferred from the gel to a PVDF membrane
317 overnight at 55V at 4°C. Membranes were blocked in either 5% dry milk or 5% BSA in

318 PBS for one hour and incubated in primary antibody overnight at 4°C. Membranes are
319 then incubated in HRP-conjugated secondary antibodies at room temperature for one
320 hour. ECL reagent (GE Healthcare) was then applied and subsequent images were
321 captured on a LI-COR Odyssey Fc Imaging System. For quantification of protein levels
322 of target proteins, β-tubulin was used as a normalization control (n=3 mice per genotype).

323 ***In Situ* hybridization** – *In situ* hybridization was conducted using RNAscope Multiplex
324 Fluorescent Reagent Kit v2 (Advanced Cell Diagnostics #323110) according to
325 manufacturer protocols for fixed, frozen tissue sample preparation protocol (ACD TN
326 320535 Rev A, 323100-USM). Briefly, 15um frozen sections were washed briefly in PBS,
327 boiled for 5 minutes in 1x Target Retrieval buffer, followed by two brief washes in $ddH_2O$
328 and one in 95% EtOH. Slides were dried then dammed with an ImmEdge hydrophobic
329 barrier pen, then incubated with Protease III for 15 minutes at 40°C. Slides were washed
330 briefly in $ddH_2O$, then incubated at 40°C in sequence with Probe-Mm-Lgr5 (312171) or or
331 Mm-Lrig3 probe (310541) (2hr), AMP 1 (30 min), AMP 2 (30 min), AMP 3 (15 min), HRP-
332 C1 (15 min), Opal-570 TSA (30 min, 1:1000), with two two-minute washes with 1x Wash
333 Buffer between hybridization steps. Slides were counterstained with DAPI and mounted
334 with N-propyl gallate mounting medium.

335 **Fluorescence microscopy: image acquisition and analysis** – Images for
336 quantification of all immunofluorescent and RNAscope images were obtained using a
337 Nikon Eclipse/Ds-Ri2 and NIS Elements software tools. Lrig3 antibody was visualized
338 using confocal microscopy on a Zeiss LSM-880 system. Images were false-colored in
339 Adobe Photoshop. All image analysis and quantification was performed in a double-blind
340 fashion and statistical comparisons were analyzed using GraphPad Prism software.

341 Quantification of all images (total “n” and counting metrics) are designated in each figure
342 legend, however there were two sets of images analyzed with different criteria and we
343 explain them here. For the quantification of *Lgr5* expression, images were acquired and
344 binned according to low- (<6 puncta per cell), mid- (6-14 puncta per cell), and high (15<
345 puncta per cell) expression levels. Example images are shown in Fig. 3*E*. For Reg4
346 quantification, we separated each colonic crypt in half (upper and lower regions) and
347 counted the positive cells in each region. Example images are shown in Fig. *H* and *J*, with
348 the dotted white line separating upper from lower.

349 **Figure Legends**

350 **Figure 1. Lrig3 expression in the colonic epithelium**. A. Schematic depicting knockout
351 of exons 4-12 in the *Lrig3*$^{-/-}$ mice, compared to WT mice. Blue antibody drawing indicates
352 where Lrig3 antibody (panels F, G-J) antigen is located. Blue line indicates where *Lrig3*
353 RNA SCOPE probe (panels B-E) is located. B-C. Representative epifluorescence RNA
354 SCOPE images of colonic tissue cross sections indicating *Lrig3* transcripts (green) are
355 located largely within the colonic epithelial compartment in wildtype mice. In *Lrig3*$^{-/-}$ mice
356 (D-E), RNA SCOPE signal (green) is lost (n=3 mice/genotype, 16 images/mouse). F.
357 Western blot comparing Lrig3 antibody reactivity in wildtype and *Lrig3*$^{-/-}$ colonic epithelial
358 cell isolation lysates (n=3). G-J. Representative images from a single confocal slice
359 illustrating Lrig3 antibody reactivity with wildtype (G-H) colonic tissue (green) cross-
360 sections (n=3 mice/genotype, 10 images/mouse). Background fluorescence observed in
361 Lrig3$^{-/-}$ (I-J). Scale bars indicate 50um. Nuclei in B-E and G-J are depicted in magenta. B,
362 D, G and H are single channel representations of the green color shown in C, E, H and J,
363 respectively.

364 **Figure 2. *Lrig3*$^{-/-}$ mice have expanded mucosal area**. A. Scatter plot indicating adult
365 *Lrig3*$^{-/-}$ mice have significantly longer colons, as measured from cecum to rectum,
366 compared to wildtype mice (n=10 mice/genotype). B. Scatter plot indicating adult *Lrig3*$^{-/-}$
367 mice have significantly more mucosal area in their colon, compared to wildtype mice (n=4,
368 10 images/mouse). C-D. Representative colon cross sections of wildtype and *Lrig3*$^{-/-}$ mice
369 that have been stained with hematoxylin and eosin. Dashed line indicates the area
370 measured for mucosal area. E. Scatter plot indicating adult *Lrig3*$^{-/-}$ mice have more nuclei
371 per crypt compared to WT mice (n=4 mice/genotype, 10 images/mouse). F. Scatter plot
372 indicating no significant change in proliferation (Ki67) between *Lrig3*$^{-/-}$ and wildtype mice
373 (n=4 mice/genotype, 10 images/mouse, 152 crypts/genotype). G-J. Representative
374 images of colonic tissue sections with anti-Ki67 antibody reactivity in *Lrig3*$^{-/-}$ (I-J) and
375 wildtype (G-H) adult animals. Nuclei in H and J are depicted in magenta. In all plots, error
376 bars indicate standard deviation from the mean. Significance was determined using an
377 unpaired t-test where a significant difference between the groups is represented by an
378 asterisk (*) when $p<0.05$. When $p<.01$., the data have been labeled with two asterisks
379 (**), and by (****) when $p<0.0001$. Scale bar in C-D indicates 50um. All breaks in the Y
380 axes are shown with parallel lines. G and I are single channel representations of the green
381 color shown in H and J, respectively.
382 **Figure 3. Expansion of the stem cell niche.** A-D. Representative RNA SCOPE images
383 of colonic tissue cross sections indicating *Lgr5* transcripts (green) between wildtype (A-
384 B) and *Lrig3*$^{-/-}$ (C-D) mice. E. Representative images of low, mid, and high *Lgr5+* transcript
385 expression. F. Scatter plot indicating *Lrig3*$^{-/-}$ mice have significantly more *Lgr5*$^{+}$ mid and
386 high cell transcript expression compared to wildtype mice (n=3 mice/genotype, 4

387 images/mouse). G-J. Representative images of colonic tissue sections comparing
388 expression of Reg4 antibody reactivity. Dotted line depicts the center of the crypt where
389 they were marked and quantified crypt upper half and lower half. K. Scatter plot indicating
390 an increase in Reg4+ cells, in the lower half of the colonic crypt, in *Lrig3*$^{-/-}$ mice compared
391 to wildtype mice (n=7 mice/genotype, 7 images/mouse). L. Scatter plot indicating no
392 change in Reg4+ cells in the upper portion of the colonic crypt of Lrig3$^{-/-}$ mice compared
393 to wildtype mice (n=7 mice/genotype, 7 images/mouse). Nuclei in B-E are depicted in
394 magenta. Scale bar indicates 50um. In all plots, error bars indicate standard deviation
395 from the mean. Significance was determined using an unpaired t-test where a significant
396 difference between the groups is represented by an asterisk (*) when $p<0.05$. When
397 $p<.01$., the data have been labeled with two asterisks (**), when $p<0.0001$, the data have
398 been labeled with four asterisks (****). A, C, G and I are single channel representations
399 of the green color shown in B, D, H and J, respectively.

400

401 **Figure 4. Expression of Lrig1 is expanded in *Lrig3*$^{-/-}$ mice.** A-D. Representative
402 images of colonic tissue sections comparing the expression of Lrig1 between wildtype (A-
403 B) and *Lrig3*$^{-/-}$ (C-D) mice. In A and C, Lrig1 (white) is detected at the cell membrane of
404 cells located in the crypt base. In B and D, Lrig1 (green) is shown in the context of all cells
405 in the crypt (magenta). E. Scatter plot indicating significantly more Lrig1$^{+}$ cells in the
406 colonic crypt of Lrig3$^{-/-}$ mice compared to wildtype (n=4 mice/genotype, 10
407 images/mouse). F. Western blot comparing Lrig1 antibody reactivity in wildtype and *Lrig3*$^{-}$
408 $^{/-}$ colonic tissue cell lysates (n=3). G-J. Representative images of colonic tissue sections
409 comparing the expression of pEgfr (I and J, green) and Egfr (G-H, green) between

410 wildtype and *Lrig3*$^{-/-}$ mice. K. Representative western blots comparing protein expression
411 for Egfr, Erk1/2, and pErk1/2 in wildtype and *Lrig3*$^{-/-}$ colonic tissue cell lysates (n=3).
412 Nuclei in G-J are depicted in magenta. Scale bars indicate 50um. Significance in scatter
413 plot was determined using an unpaired t- test where a significant difference between the
414 groups is represented by an asterisk (****) when $p<0.0001$. A and C are single channel
415 representations of the green color shown in B and D respectively.

416

417 **Supplemental Figure 1. Wildtype and Lrig3$^{-/-}$ allele map, sequence, and PCR**
418 **screening of mice.** A-B. Schematic representation of the wildtype and *Lrig3*$^{-/-}$ genes.
419 Disruption of *Lrig3* was achieved through the removal of exons 4-12, joining the third and
420 twelfth intron. B. The intervening remaining sequence (650bp) is shown. C. Confirmatory
421 PCR analysis of the wildtype *Lrig3* allele, using primers that are located upstream (5') and
422 downstream (3') of the fourth exon, and generate 1.2kb PCR product. *Lrig3*$^{-/-}$ mice do not
423 generate a PCR product, as they lack the 3' site. D. Confirmatory PCR analysis of the null
424 *Lrig3* allele, using primers that are located upstream (5') of the fourth exon and
425 downstream (3') of the twelfth exon, generates a 650bp product in the null mice. Wildtype
426 mice do not generate a PCR product under standard conditions, as that region is 10kb in
427 length. *Lrig3* mutant heterozygous and homozygous mice are viable and fertile. PCR
428 primer sequences are listed in Supplemental Table 1.

429 **Supplemental Figure 2. Differentiated Cell marker expression in *Lrig3*$^{-/-}$ and**
430 **wildtype colons.** A-D**.** Representative images of Vil-1 expression (green) in the
431 absorptive cells of the colonic epithelium in wildtype (A-B) *Lrig3*$^{-/-}$ colons (C-D). B' and D'.
432 Enlarged images of Vil-1 expression shown in wildtype (B and B') and *Lrig3*$^{-/-}$ (D and D').

433 E-H. Representative images of Dclk1 expression (green) in tuft cells of colonic epithelium
434 in wildtype (E-F) *Lrig3*$^{-/-}$ (G-H) colons. I. Scatter plot indicating no significant change in
435 Dclk1$^{+}$ cells in the colonic crypts of *Lrig3*$^{-/-}$ compared to wildtype mice (n=4, 10
436 images/mouse). J-M. representative images of ChgA expression (green) in
437 neuroendocrine cells of the colonic epithelium in wildtype (J-K) and *Lrig3*$^{-/-}$ (L-M) colons.
438 N. Scatter plot indicating no significant change in ChgA$^{+}$ cells in the colonic epithelium of
439 *Lrig3*$^{-/-}$ compared to wildtype mice (n=4, 10 images/mouse). For both panels, nuclei in are
440 depicted in magenta and the scale bar indicates 50um.

441

442

443 **Supplemental Table 1**

| **WT and *Lrig3*$^{-/-}$ primers** | |
|---|---|
| WT & *Lrig3*$^{-/-}$ 5' primer | 5' gctaaagcagccacagagtggta 3' |
| WT 3' primer | 5' ctgtgccctcaaactgtcaa 3' |
| *Lrig3*$^{-/-}$ 3' primer | 5' ttccctggactggtaggtagctc 3' |

444

445 **Supplemental Table 2**

| Antibody | Company | Product# | Concentration |
|---|---|---|---|
| Lrig3 | US Biological | 151911 | 1:250(IF)<br>1:300 (WB) |
| Lrig1 | R&D Systems | AF3688 | 1:500 (IF)<br>1:300 (WB) |
| Ki67(PE) | eBiosciences | SolA15 | 1:100 (IF) |
| Egfr | abcam | ab52894 | 1:500 (IF)<br>1:1000(WB) |

| | | | |
|---|---|---|---|
| pEgfr (Y1068) | abcam | 200709 | 1:400 (IF) |
| Erk | Bioss | BS-0022R | 1:1000 (WB) |
| pErk | Cell Signaling Technology | 4370S | 1:1000 (WB) |
| Reg4 | R&D Systems | AF1379 | 1:100 (IF) |

446

447 **References**


448 1. **Abousoliman I**, **Reyer H**, **Oster M**, **Murani E**, **Mohamed I**, **Wimmers K**.
449 Genome-Wide Analysis for Early Growth-Related Traits of the Locally Adapted
450 Egyptian Barki Sheep. *Genes (Basel)* 12, 2021. doi: 10.3390/genes12081243.

451 2. **Abraira VE**, **del Rio T**, **Tucker AF**, **Slonimsky J**, **Keirnes HL**, **Goodrich L V**.
452 Cross-repressive interactions between Lrig3 and Netrin1 shape the architecture of
453 the inner ear. *Development* 135: 4091–4099, 2008. doi: 10.1242/dev.029330.

454 3. **Abraira VE**, **Satoh T**, **Fekete DM**, **Goodrich L V.** Vertebrate Lrig3-ErbB
455 interactions occur in vitrobut are unlikely to play a role in Lrig3-dependent inner
456 ear morphogenesis. *PLoS One* 5, 2010. doi: 10.1371/journal.pone.0008981.

457 4. **Barker N**, **van Es JH**, **Kuipers J**, **Kujala P**, **van den Born M**, **Cozijnsen M**,
458 **Haegebarth A**, **Korving J**, **Begthel H**, **Peters PJ**, **Clevers H**. Identification of
459 stem cells in small intestine and colon by marker gene Lgr5 [Online]. *Nature* 449:
460 1003, 2007. http://dx.doi.org/10.1038/nature06196.

461 5. **Cai MJ**, **Xie RF**, **Han L**, **Chen RD**, **Wang BF**, **Ye F**, **Guo DS**, **Lei T**. Effect of
462 RNAi-mediated LRIG3 gene silencing on proliferation of glioma GL15 cells and
463 expression of PCNA and Ki-67. *Chin J Cancer* 28: 1–4, 2009.

464 6. **Chen Y**, **Wang Q**, **Wang M**, **Li M**. Overexpressed LRIG3 gene ameliorates
465 prostate cancer through suppression of cell invasion and migration. *Int J Biol*
466 *Macromol* 124: 1–9, 2019. doi: https://doi.org/10.1016/j.ijbiomac.2018.11.028.

467 7. **De Vincenti AP**, **Alsina FC**, **Ferrero Restelli F**, **Hedman H**, **Ledda F**, **Paratcha**
468 **G**. Lrig1 and Lrig3 cooperate to control Ret receptor signaling, sensory axonal
469 growth and epidermal innervation. *Development* 148, 2021. doi:
470 10.1242/dev.197020.

471 8. **del Rio T**, **Nishitani AM**, **Yu W-M**, **Goodrich L V**. In Vivo Analysis of Lrig Genes
472 Reveals Redundant and Independent Functions in the Inner Ear [Online]. *PLOS*
473 *Genet* 9: e1003824, 2013. https://doi.org/10.1371/journal.pgen.1003824.

474 9. **Dessimoz J**, **Opoka R**, **Kordich JJ**, **Grapin-Botton A**, **Wells JM**. FGF signaling
475 is necessary for establishing gut tube domains alongthe anterior–posterior axis in
476 vivo. *Mech Dev* 123: 42–55, 2006. doi: https://doi.org/10.1016/j.mod.2005.10.001.

477 10. **Gehart H**, **Clevers H**. Tales from the crypt: new insights into intestinal stem cells.

*Nat Rev Gastroenterol Hepatol* 16: 19–34, 2019. doi: 10.1038/s41575-018-0081-y.

11. **Hellström M**, **Ericsson M**, **Johansson B**, **Faraz M**, **Anderson F**, **Henriksson R**, **Nilsson SK**, **Hedman H**. Cardiac hypertrophy and decreased high-density lipoprotein cholesterol in Lrig3-deficient mice [Online]. *Am J Physiol - Regul Integr Comp Physiol* 310: R1045, 2016. http://ajpregu.physiology.org/content/310/11/R1045.abstract.

12. **Hu X**, **Zhou K**, **Cao S**, **Zhu H**, **Xie K**. Circ_lrig3 contributes to the progression of hepatocellular carcinoma by elevating rnf38 via sponging mir-449a. *Gen Physiol Biophys* 40, 2021. doi: 10.4149/gpb_2020044.

13. **Kwon O**, **Han T-S**, **Son M-Y**. Intestinal Morphogenesis in Development, Regeneration, and Disease: The Potential Utility of Intestinal Organoids for Studying Compartmentalization of the Crypt-Villus Structure. *Front cell Dev Biol* 8: 593969, 2020. doi: 10.3389/fcell.2020.593969.

14. **Liu P**, **Jenkins NA**, **Copeland NG**. A highly efficient recombineering-based method for generating conditional knockout mutations. *Genome Res* 13: 476–484, 2003. doi: 10.1101/gr.749203.

15. **Metodiev S**, **Thekkoot DM**, **Young JM**, **Onteru S**, **Rothschild MF**, **Dekkers JCM**. A whole-genome association study for litter size and litter weight traits in pigs. *Livest Sci* 211, 2018. doi: 10.1016/j.livsci.2018.03.004.

16. **Osaki LH**, **Gama P**. MAPKs and Signal Transduction in the Control of Gastrointestinal Epithelial Cell Proliferation and Differentiation. *Int J Mol Sci* 14: 10143–10161, 2013. doi: 10.3390/ijms140510143.

17. **Peng C**, **Chen H**, **Li Y**, **Yang H**, **Qin P**, **Ma B**, **Duan Q**, **Wang B**, **Mao F**, **Guo D**. LRIG3 Suppresses Angiogenesis by Regulating the PI3K/AKT/VEGFA Signaling Pathway in Glioma. *Front Oncol* 11: 54, 2021. doi: 10.3389/fonc.2021.621154.

18. **Powell AE**, **Wang Y**, **Li Y**, **Poulin EJ**, **Means AL**, **Washington MK**, **Higginbotham JN**, **Juchheim A**, **Prasad N**, **Levy SE**, **Guo Y**, **Shyr Y**, **Aronow BJ**, **Haigis KM**, **Franklin JL**, **Coffey RJ**. The pan-ErbB negative regulator, Lrig1, is an intestinal stem cell marker that functions as a tumor suppressor. *Cell* 149: 146–158, 2012. doi: 10.1016/j.cell.2012.02.042.

19. **Qiu Y**, **Han Q**, **Lu H**, **Shi C**. miR-196a targeting LRIG3 promotes the proliferation and migration of cervical cancer cells. *Cell Mol Biol* 66, 2020. doi: 10.14715/cmb/2020.66.7.27.

20. **Sasaki N**, **Sachs N**, **Wiebrands K**, **Ellenbroek SIJ**, **Fumagalli A**, **Lyubimova A**, **Begthel H**, **Van Born M Den**, **Van Es JH**, **Karthaus WR**, **Li VSW**, **López-Iglesias C**, **Peters PJ**, **Van Rheenen J**, **Van Oudenaarden A**, **Clevers H**. Reg4+ deep crypt secretory cells function as epithelial niche for Lgr5+ stem cells in colon. *Proc Natl Acad Sci U S A* 113: E5399–E5407, 2016. doi: 10.1073/pnas.1607327113.

518 21. **Schlieve CR**, **Mojica SG**, **Holoyda KA**, **Hou X**, **Fowler KL**, **Grikscheit TC**.
519 Vascular Endothelial Growth Factor (VEGF) Bioavailability Regulates
520 Angiogenesis and Intestinal Stem and Progenitor Cell Proliferation during
521 Postnatal Small Intestinal Development [Online]. *PLoS One* 11: e0151396, 2016.
522 https://doi.org/10.1371/journal.pone.0151396.

523 22. **Simion C**, **Prieto MEC**, **Sweeney C**. The LRIG family – enigmatic regulators of
524 growth factor receptor signaling. *Endocr Relat Cancer* 21: R431–R443, 2014. doi:
525 10.1530/ERC-14-0179.

526 23. **Sun H**, **Zhai J**, **Zhang L**, **Chen Y**. CircRNA LRIG3 knockdown inhibits
527 hepatocellular carcinoma progression by regulating miR-223-3p and MAPK/ERK
528 pathway. .

529 24. **Sun S**, **Gao J**, **Zhou S**, **Li Y**, **Wang Y**, **Jin L**, **Li J**, **Liu B**, **Zhang B**, **Han S**, **Ding**
530 **H**, **Li X**. A novel circular RNA circ-LRIG3 facilitates the malignant progression of
531 hepatocellular carcinoma by modulating the EZH2/STAT3 signaling. *J Exp Clin*
532 *Cancer Res* 39: 252, 2020. doi: 10.1186/s13046-020-01779-5.

533 25. **Wang Y**, **Shi C**, **Lu Y**, **Poulin EJ**, **Franklin JL**, **Coffey RJ**. Loss of Lrig1 leads to
534 expansion of Brunner glands followed by duodenal adenomas with gastric
535 metaplasia. *Am J Pathol* 185: 1123–34, 2015. doi: 10.1016/j.ajpath.2014.12.014.

536 26. **Wong VWY**, **Stange DE**, **Page ME**, **Buczacki S**, **Wabik A**, **Itami S**, **van de**
537 **Wetering M**, **Poulsom R**, **Wright NA**, **Trotter MWB**, **Watt FM**, **Winton DJ**,
538 **Clevers H**, **Jensen KB**. Lrig1 controls intestinal stem cell homeostasis by
539 negative regulation of ErbB signalling. *Nat Cell Biol* 14: 401–408, 2012. doi:
540 10.1038/ncb2464.

541 27. **Yui S**, **Azzolin L**, **Maimets M**, **Pedersen MT**, **Fordham RP**, **Hansen SL**, **Larsen**
542 **HL**, **Guiu J**, **Alves MRP**, **Rundsten CF**, **Johansen J V**, **Li Y**, **Madsen CD**,
543 **Nakamura T**, **Watanabe M**, **Nielsen OH**, **Schweiger PJ**, **Piccolo S**, **Jensen KB**.
544 YAP/TAZ-Dependent Reprogramming of Colonic Epithelium Links ECM
545 Remodeling to Tissue Regeneration. *Cell Stem Cell* 22: 35-49.e7, 2018. doi:
546 10.1016/j.stem.2017.11.001.

547 28. **Zeng K**, **Chen X**, **Xu M**, **Liu X**, **Li C**, **Xu X**, **Pan B**, **Qin J**, **He B**, **Pan Y**, **Huiling**
548 **S**, **Xu T**, **Wang S**. LRIG3 represses cell motility by inhibiting slug via inactivating
549 ERK signaling in human colorectal cancer. *IUBMB Life* : 1–11, 2020. doi:
550 10.1002/iub.2262.

551 29. **Zeng K**, **Chen X**, **Xu M**, **Liu X**, **Li C**, **Xu X**, **Pan B**, **Qin J**, **He B**, **Pan Y**, **Huiling**
552 **S**, **Xu T**, **Wang S**. LRIG3 represses cell motility by inhibiting slug via inactivating
553 ERK signaling in human colorectal cancer. *IUBMB Life* : 1–11, 2020. doi:
554 10.1002/iub.2262.

555 30. **Zhao H**, **Tanegashima K**, **Ro H**, **Dawid IB**. Lrig3 regulates neural crest formation
556 in Xenopus by modulating Fgf and Wnt signaling pathways. *Development* 135:
557 1283–1293, 2008. doi: 10.1242/dev.015073.

558 31. **Zhou H**, **Cao J**, **Yang F**, **Fan D**, **Li H**, **Fan T**, **Sun P**. Member Domain 3 (LRIG3)

559 Activates Hypoxia-Inducible Factor-1 α /Vascular Endothelial Growth Factor (HIF-
560 1 α /VEGF) Pathway to Inhibit the Growth of Bone Marrow Mesenchymal Stem
561 Cells in Glioma . *J Biomater Tissue Eng* 11, 2021. doi: 10.1166/jbt.2021.2629.

562 32. Genepaint [Online]. [date unknown]. https://gp3.mpg.de.

563

564

565

Figure 1

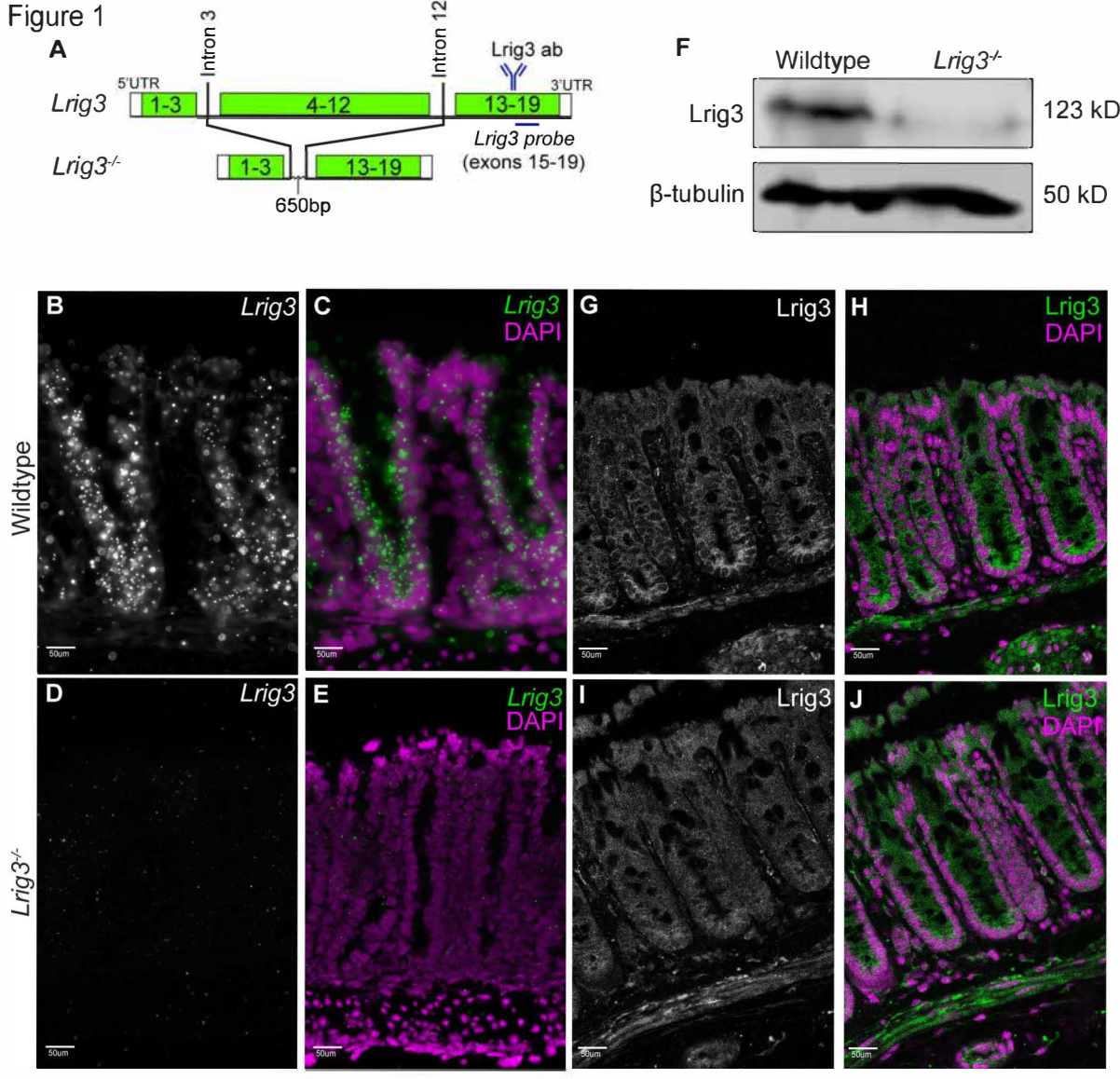
A
Intron 3
Intron 12
Lrig3 ab
5'UTR
3'UTR
Lrig3
1-3
4-12
13-19
Lrig3 probe
(exons 15-19)
Lrig3-/-
1-3
13-19
650bp
F
Wildtype
Lrig3-/-
Lrig3
123 kD
β-tubulin
50 kD
B
Lrig3
C
Lrig3
DAPI
G
Lrig3
H
Lrig3
DAPI
Wildtype
D
Lrig3
E
Lrig3
DAPI
I
Lrig3
J
Lrig3
DAPI
Lrig3-/-
50um

Figure 2

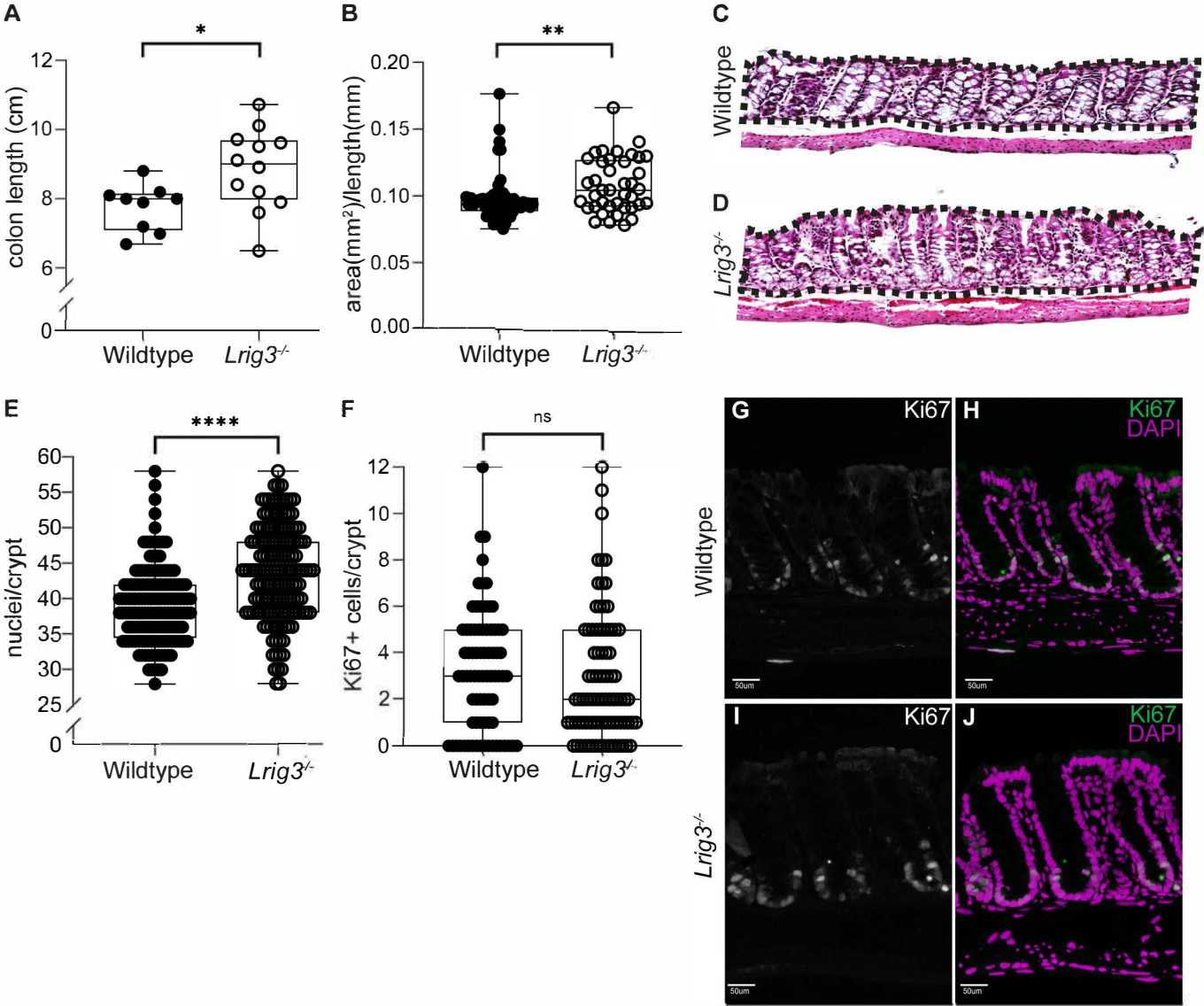
A
*
colon length (cm)
12
10
8
6
0
Wildtype
Lrig3-/-
B
**
area(mm²)/length(mm)
0.20
0.15
0.10
0.05
0.00
Wildtype
Lrig3-/-
C
Wildtype
D
Lrig3-/-
E
****
nuclei/crypt
60
55
50
45
40
35
30
25
0
Wildtype
Lrig3-/-
F
ns
Ki67+ cells/crypt
12
10
8
6
4
2
0
Wildtype
Lrig3-/-
G
Ki67
H
Ki67
DAPI
Wildtype
50um
I
Ki67
J
Ki67
DAPI
Lrig3-/-
50um

Figure 3

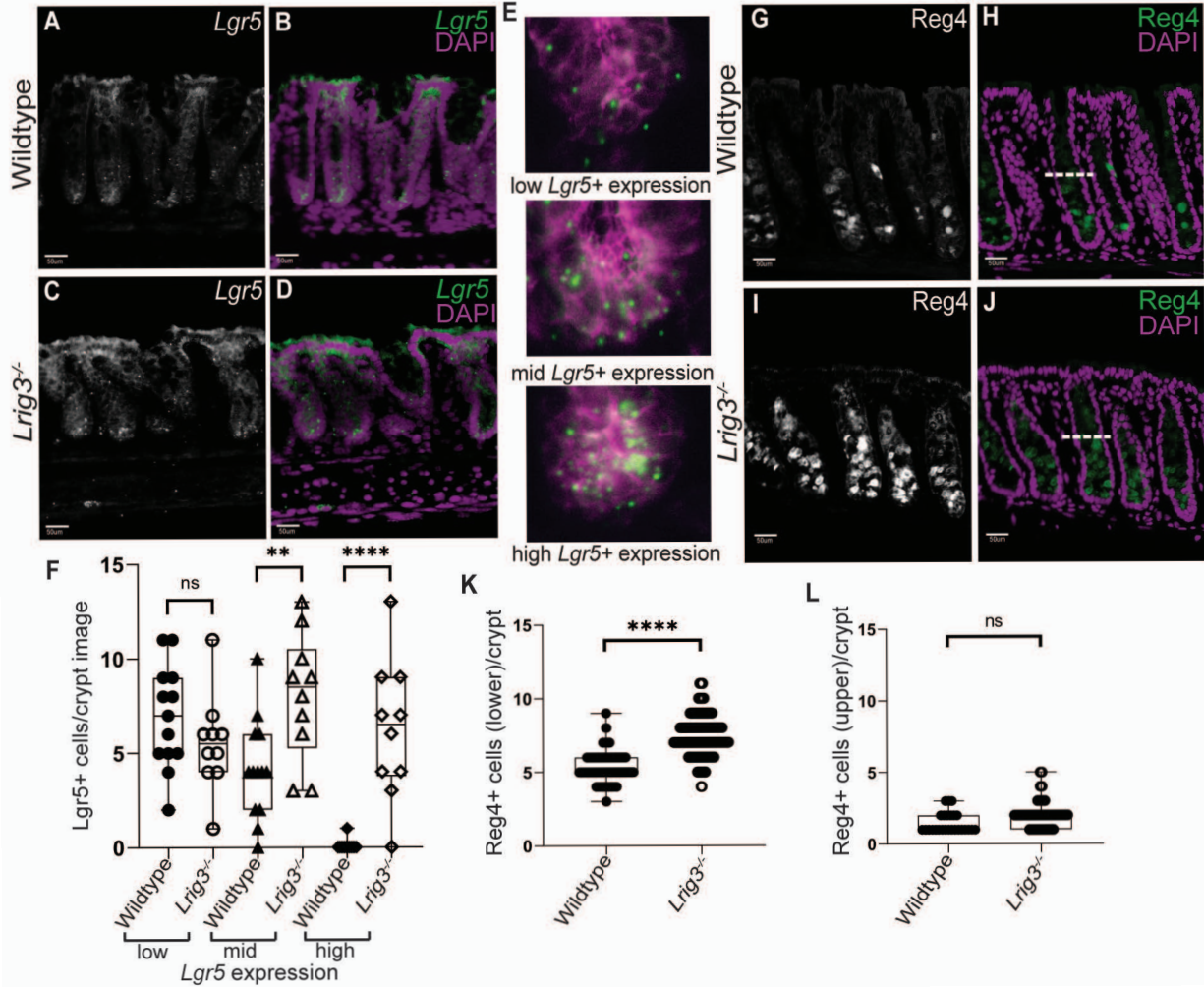
A
Lgr5
B
Lgr5
DAPI
Wildtype
C
Lgr5
D
Lgr5
DAPI
Lrig3-/-
E
low Lgr5+ expression
mid Lgr5+ expression
high Lgr5+ expression
G
Reg4
H
Reg4
DAPI
Wildtype
I
Reg4
J
Reg4
DAPI
Lrig3-/-
F
Lgr5+ cells/crypt image
ns
**
****
Wildtype
Lrig3-/-
low
mid
high
Lgr5 expression
K
Reg4+ cells (lower)/crypt
****
Wildtype
Lrig3-/-
L
Reg4+ cells (upper)/crypt
ns
Wildtype
Lrig3-/-

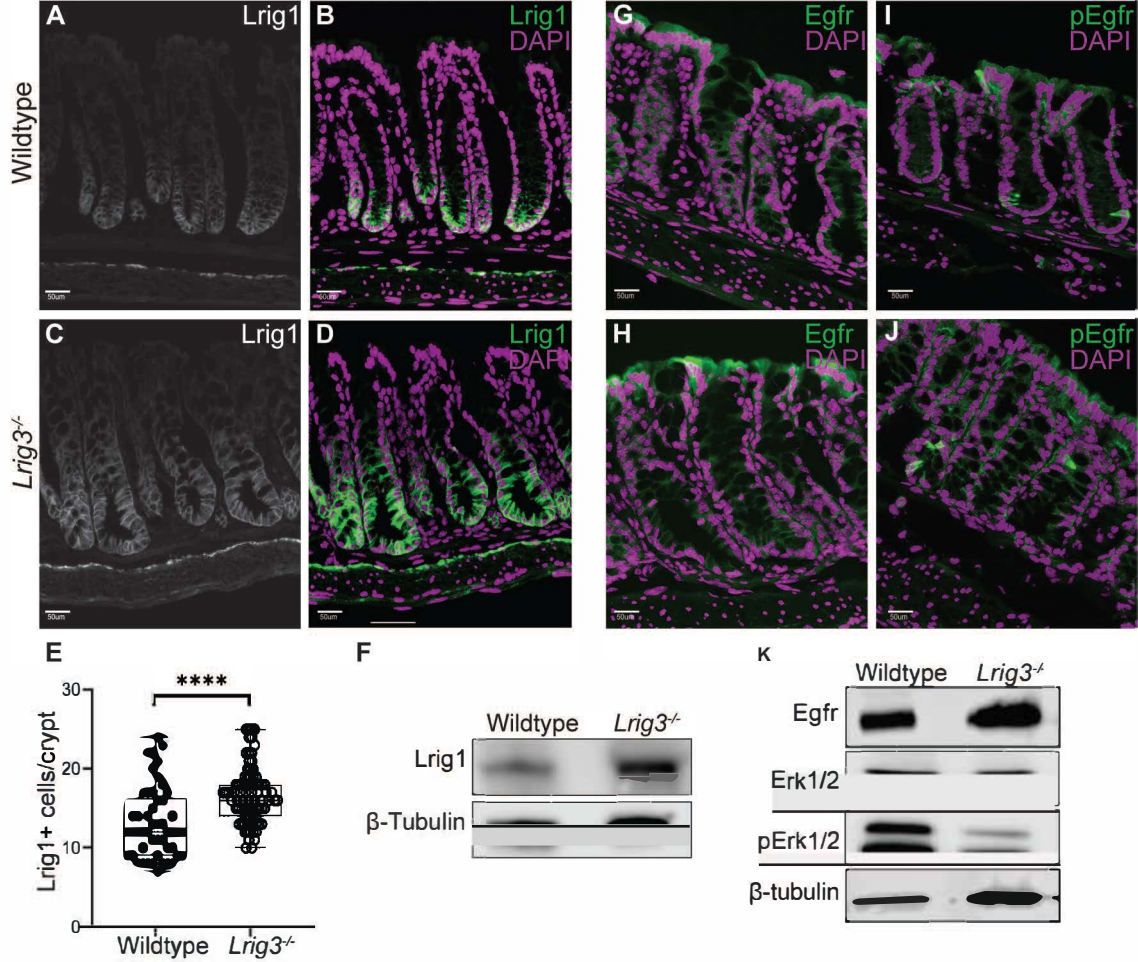
A
Lrig1
B
Lrig1
DAPI
G
Egfr
DAPI
I
pEgfr
DAPI
Wildtype
C
Lrig1
D
Lrig1
DAPI
H
Egfr
DAPI
J
pEgfr
DAPI
Lrig3-/-
50um
E
****
Lrig1+ cells/crypt
30
20
10
0
Wildtype
Lrig3-/-
F
Wildtype
Lrig3-/-
Lrig1
β-Tubulin
K
Wildtype
Lrig3-/-
Egfr
Erk1/2
pErk1/2
β-tubulin